Stability of the Oil-Air Boundary in Fluid Dynamic Bearings of Hard Disk Drives. The Hitachi Problem from MPI 2005

May 23, 2006

Industrial Representative: F. Hendriks (Hitachi)

Faculty: B.S. Tilley (Olin College), C.P. Please (Southampton, UK), J. Billingham (Nottingham, UK), P. Dellar (Imperial College, UK), C. Breward (Oxford, UK), C.S. Raymond (NJIT), D. Schwendeman (RPI), J.D. Fehribach (WPI)

Students: A.S. Ball (Delaware), L.J. Jones (Cal. St. East Bay), A. Chakrabortty (RPI), C.C. Boughan (RPI), K.W. Johnson (RPI), J. Phillips (McGill), D. Badamdorj (U. Cincinatti)

1 Introduction

Recently, the use of fluid dynamic bearing spindle motors in hard-disk drive applications has been widespread, due to lowering acoustical noise, minimizing Non Repeatable Runout (NRRO) and improving reliability [1]. Figure 1a shows a schematic of a sample disk drive, and a cross-section of the spindle (or stator) and the rotor. Typical spatial dimensions are shown in the figure. Characteristic rotation rates for server drives are between 10,000 and 15,000 rpm, while laptop drives may be 4,500 rpm. The focus of this report is the stability of the meniscus region during operation. Note that the spindle and stator have smooth surfaces, unlike those found near the bearing region (see the MPI 2004 report for more information, or [3]). For this report, we assume that any disturbance pressures from the fluid-dynamic bearing region are neglible.

Note from Table 1, hydrostatic pressures are small compared to the capillary pressures (e.g. $Bo \approx 50$). Hence, the tilt of the axis, as shown in Figure 1, need not be considered. We investigated two different geometries: the slot problem (see Figure 1b) and the cylindrical problem (see Figure 1c). The slot problem consists to parallel plates of infinite extent (compared to the gap thickness). A plane Couette flow is driven with one plate moving perpendicularly to the plane of Figure 1b, and we consider the stability of this configuration in the limit of zero Reynolds number.

The inviscid limit of this case has been considered by [4]. In this limit, viscous normal and tangential stresses are ignored, and any contact-line dynamics need not be considered. Figure 2 (Fig. 2 from [4]) shows the stability of an inviscid disturbance of a flat interface base state with Couette flow. Note that in the limit of interest here, the critical wavenumber of the disturbance centers near $k \approx 6$, and based on the Froude number of the system, a wide band of unstable modes is possible under normal operation. However, the inviscid analysis needs to neglect tangential stresses at the fluid boundaries, so that wettability effects and viscous stresses are neglected. In this application, they appear to play a significant, if not dominant role. In the work that follows, we consider the $Re \to 0$ limit, and find that this system remains stable for all of the eigenvalues found. Our analysis includes finite contact-angle effects near the trijunctions.

The second geometry to be considered in a cylindrical geometry (see Figure 1c). An inviscid analysis, similar to that of [4] for the Cartesian case, results in a spatially nonuniform base-state interfacial profile, since the centrifugal terms in the momentum equations result in a nontrivial pressure distribution. This shape is governed by

$$\frac{Fr}{Bo}\frac{v^2}{r} \approx -\frac{\partial}{\partial r}\left\{\kappa\right\} \ , \tag{1}$$

where v is the azimuthal component of the fluid velocity at the interface, r is the radial variable, and κ is twice the mean curvature of the interface[1]. In fact, two-fluid systems in a Taylor-Couette device appear to arrange themselves into density stratified layers due to this pressure distribution [5, 6]. In the analysis below, we considered only the small-gap limit in the zero Reynolds number case. From this limit, we found that again, all of the azimuthal disturbances appear to be stable.

The report is organized in the following manner. In Section 2, we develop the linear stability theory for the OAI problem in a Cartesian, or slot geometry. From this analysis, we find that for finite capillary numbers, two neutrally stable modes appear independent of the wavenumber. In Section 3, we develop the linear stability problem in the cylindrical geometry in the small gap limit (where the gap thickness is much smaller than the radius of the inner cylinder). We find that this reduced model, in the limit of zero Reynolds number, reproduces the stability problem found in Section 2 in the limit of zero wavenumber. In both of these models, if we consider the limit of zero wavenumber but scale the capillary number of the gap thickness. In both cases, the system appears to be stable for vanishingly small Reynolds numbers. We discuss the results of this analysis in the final section.

2 Slot Geometry

Here we consider the following problem: an incompressible viscous fluid (the 'oil') is confined to the infinite slot between two vertical side walls, one stationary, one moving. The fluid does not entirely fill the slot. The domain occupied by the fluid is bounded above by a free surface located at $z = F(x, y, t)$, while it is unbounded from below. We use a Cartesian coordinate system, oriented so that the fluid meets the stationary side wall at $x = 0$. The moving wall is translating along the slot in the y direction at speed U. Above the oil, there is a second fluid in the slot (the 'air'), which is assumed to be passive, in the sense that its only effect on the problem describing the motion of the oil is to set a constant pressure at the free surface.

We use the incompressible Navier-Stokes equations to describe the motion of the fluid. In vector form, we have:

$$\nabla \cdot \mathbf{u} = 0. \tag{2}$$

$$\rho\left\{\frac{\partial \mathbf{u}}{\partial t} + (\mathbf{u}\cdot\nabla)\mathbf{u}\right\} = -\nabla p + \mu\nabla^2\mathbf{u} + \rho\mathbf{g}, \tag{3}$$

The boundary conditions are the no-slip boundary conditions along the walls[2],

$$\underline{x = 0} : u = v = w = 0 \ , \ \underline{x = d} : u = w = 0, v = U_o \ .$$

In addition, we assume that the flow far from the interface approaches Taylor-Couette flow

$$\underline{z \to -\infty} : u, w \to 0 \ , v \to U_o x/d \ .$$

[1]The derivation of this relation can be found in the appendix.

[2]The nonintegrable stress singularity at the contact lines will be addressed in a later section

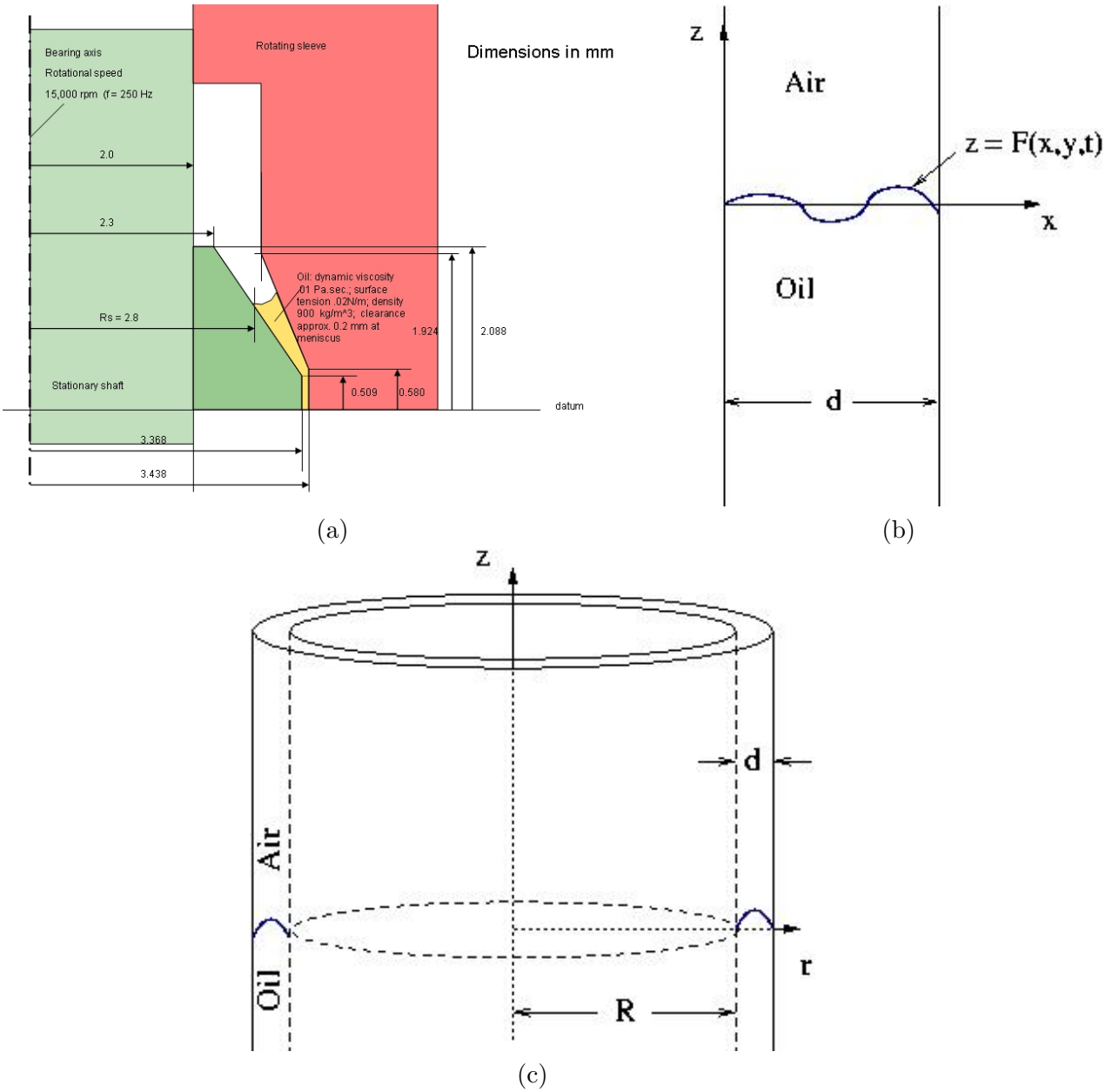

Figure 1: (a) Capillary buffer region about the fluid bearing in a hard disk drive. (b) Slot geometry. (c) Cylindrical geometry.

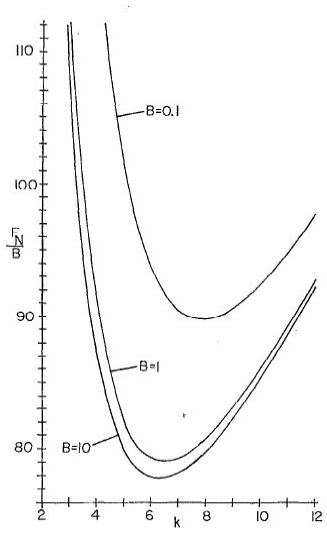

Figure 2: From [4], Fig. 2. Neutral stability curves for the inviscid slot problem. B corresponds to our Bond number Bo, while F_N corresponds to the neutral value of the Froude number Fr. From this diagram, the slot geometry (see Figure 1b) is unstable over a range of wavenumbers k.

Dimensional quantities		Dimensionless quantities	
Gap thickness d	200 μm	Aspect Ratio	$\epsilon = d/R = 10^{-1}$
Stator radius R	2 mm		
Rotation rate Ω	15,000 rpm	Reduced Reynolds Number	$Re = \frac{\rho \Omega d^2}{\mu} = 6$
Fluid density ρ	900 kg/m^3	Froude Number	$Fr = \frac{(\Omega R)^2}{(gd)} = 4 \times 10^5$
Fluid dynamic viscosity μ	0.01 Pa· s	Capillary Number	$Ca = \frac{\mu \Omega R}{\sigma} = 1.5$
Surface tension σ	0.02 N/m	Bond Number	$Bo = \frac{\sigma}{\rho g d^2} = 50$

Table 1: Table of dimensional and dimensionless quantities.

At the free surface, we apply the kinematic boundary conditon, normal fluid stresses are balanced by capillary stresses, and that there are no applied tangential stresses to the fluid at the interface:

$$F_t + uF_x + vF_y - w = 0 \tag{4}$$

$$\begin{aligned} -p + 2\mu \mathbf{n} \cdot \mathbf{e} \cdot \mathbf{n} &= \sigma \kappa & (5) \\ [\mathbf{e} \cdot \mathbf{n}] \times \mathbf{n} &= \mathbf{0} & (6) \end{aligned}$$

where $\mathbf{e}$ is the rate-of-strain tensor of the fluid, $\mathbf{n}$ is the outward unit normal vector to the interface

$$\mathbf{n} = \frac{-F_x \mathbf{x} \; - F_y \mathbf{y} \; + \mathbf{z}}{\sqrt{1 + F_x^2 + F_y^2}} \; ,$$

σ is the surface tension of the oil, $\kappa = \nabla \cdot \mathbf{n}$ and is the mean curvature. Initially, we assume that the contact angle that the free surface makes to the walls is $\pi/2$.

We apply the following scales to the problem, using the notation $[f]$ to denote the scale,

$$[x, y, z] = d \; , \; [u, v, w] = U_o \; , \; [t] = d/U_o \; , \; [p] = \frac{\mu U_o}{d} \; , \; [F] = d \; ,$$

to find the following nondimensional version of our system

$$\frac{\partial u}{\partial x}+\frac{\partial v}{\partial y}+\frac{\partial w}{\partial z}=0\ , \tag{7}$$

$$\mathrm{Re}\left(\frac{\partial u}{\partial t}+u\frac{\partial u}{\partial x}+v\frac{\partial u}{\partial y}+w\frac{\partial u}{\partial z}\right)=-\frac{\partial p}{\partial x}+\left(\frac{\partial^2 u}{\partial x^2}+\frac{\partial^2 u}{\partial y^2}+\frac{\partial^2 u}{\partial z^2}\right), \tag{8}$$

$$\mathrm{Re}\left(\frac{\partial v}{\partial t}+u\frac{\partial v}{\partial x}+v\frac{\partial v}{\partial y}+w\frac{\partial v}{\partial z}\right)=-\frac{\partial p}{\partial y}+\left(\frac{\partial^2 v}{\partial x^2}+\frac{\partial^2 v}{\partial y^2}+\frac{\partial^2 v}{\partial z^2}\right), \tag{9}$$

$$\mathrm{Re}\left(\frac{\partial w}{\partial t}+u\frac{\partial w}{\partial x}+v\frac{\partial w}{\partial y}+w\frac{\partial w}{\partial z}\right)=-\frac{\partial p}{\partial z}+\left(\frac{\partial^2 w}{\partial x^2}+\frac{\partial^2 w}{\partial y^2}+\frac{\partial^2 w}{\partial z^2}\right)\ , \tag{10}$$

where $\mathrm{Re}=U_o d/\nu$, $\nu=\mu/\rho$ is the Reynolds number and the kinematic viscosity, respectively. The no-slip boundary conditions become

$$\underline{x=0}:\quad u=v=w=0\ ,\ \underline{x=1}:\quad u=w=0\ , v=1\ ,$$

and the far-field condition becomes

$$\underline{z\to-\infty}:\quad u,w\to 0\ , v\to x\ .$$

The interfacial conditions (4)-(6) become

$$F_t+uF_x+vF_y-w=0 \tag{11}$$

$$-p+\frac{2}{\sqrt{1+F_x^2+F_y^2}}\left\{w_z-F_y\left[v_z+w_y\right]-F_x\left[u_z+w_x\right]+F_y^2 v_y+F_x^2 u_x+2F_xF_y\left[u_y+v_x\right]\right\}=$$

$$\frac{1}{\mathrm{Ca}}\left\{\frac{F_{xx}\left(1+F_x^2\right)+F_{yy}\left(1+F_y^2\right)-2F_xF_yF_{xy}}{\left(1+F_x^2+F_y^2\right)^{3/2}}\right\}\ , \tag{13}$$

$$\begin{aligned}\left\{(u_z+w_x)\left(1-F_x^2\right)-F_y(u_y+v_x)+2F_x(w_z-u_x)-F_xF_y(v_y+w_x)\right\} &= 0 &(14)\\ \left\{(v_z+w_y)\left(1-F_y^2\right)-F_x(u_y+v_x)+2F_y(w_z-v_y)-F_yF_x(u_z+w+x)\right\} &= 0\ , &(15)\end{aligned}$$

where $\mathrm{Ca}=\mu U_o/\sigma$ is the capillary number.

2.1 Linearization around the Basic State

Note that the Couette flow $u=w=0, v=x$ solves this problem provided that $F=0$ for all x,y. We perform the linear stability theory of this problem about this state with the assumption

$$\begin{aligned}u &= \delta\left\{\hat{U}(x,z)e^{-iky+ct}+c.c.\right\} &(16)\\ v &= x+\delta\left\{\hat{V}(x,z)e^{-iky+ct}+c.c.\right\} &(17)\\ w &= \delta\left\{\hat{W}(x,z)e^{-iky+ct}+c.c.\right\} &(18)\\ p &= \delta\left\{\hat{P}(x,z)e^{-iky+ct}+c.c.\right\} &(19)\\ F &= \delta\left\{\hat{F}(x)e^{-iky+ct}+c.c.\right\} &(20)\end{aligned}$$

and substitute this into (7)-(15) and keep only the terms which are linear in δ to arrive at the linear system (for $\mathrm{Re} = 0$):

$$\hat{U}_x + \hat{W}_z - i\,k\hat{V} = 0, \tag{21}$$

$$\hat{U}_{xx} + \hat{U}_{zz} - k^2\hat{U} - \hat{P}_x = 0, \tag{22}$$

$$\hat{V}_{xx} + \hat{V}_{zz} - k^2\,\hat{V} + ik\hat{P} = 0, \tag{23}$$

$$\hat{W}_{xx} + \hat{W}_{zz} - k^2\hat{W} - \hat{P}_z = 0, \tag{24}$$

for $0 < x < 1$ and $z < 0$, subject to

$$\hat{U} = \hat{V} = \hat{W} = 0 \quad \text{at } x = 0 \text{ and } x = 1 \text{ for } z < 0, \tag{25}$$

$$\hat{U} \to 0, \quad \hat{V} \to 0, \quad \hat{W} \to 0 \quad \text{as } z \to -\infty \text{ for } 0 < x < 1, \tag{26}$$

$$-i\,k\,(x - c)\hat{F} = \hat{W} \quad \text{at } z = 0 \text{ for } 0 < x < 1, \tag{27}$$

$$\mathrm{Ca}\left(-\hat{P} + 2\hat{W}_z\right) = -\hat{F}_{xx} + k^2\hat{F} \quad \text{at } z = 0 \text{ for } 0 < x < 1, \tag{28}$$

$$\hat{V}_z = \hat{F}_x + ik\hat{W} \quad \text{at } z = 0 \text{ for } 0 < x < 1, \tag{29}$$

$$\hat{U}_z + \hat{W}_x = -ik\,\hat{F} \quad \text{at } z = 0 \text{ for } 0 < x < 1, \tag{30}$$

$$F_x = 0 \quad \text{at } z = 0,\ x = 0 \text{ and } x = 1. \tag{31}$$

2.1.1 Numerical Results

The scaled linear stability problem is

$$U_x + W_z - iV = 0, \tag{32}$$

$$U_{xx} + U_{zz} - k^2U - P_x = 0, \tag{33}$$

$$V_{xx} + V_{zz} - k^2V + ik^2P = 0, \tag{34}$$

$$W_{xx} + W_{zz} - k^2W - P_z = 0, \tag{35}$$

for $0 < x < 1$ and $z < 0$, subject to

$$U = V = W = 0 \quad \text{at } x = 0 \text{ and } x = 1 \text{ for } z < 0, \tag{36}$$

$$U \to 0, \quad V \to 0, \quad W \to 0 \quad \text{as } z \to -\infty \text{ for } 0 < x < 1, \tag{37}$$

$$k\mathrm{Ca}\,(P - 2W_z) = -F_{xx} + k^2F \quad \text{at } z = 0 \text{ for } 0 < x < 1, \tag{38}$$

$$W = (c - ix)\,F \quad \text{at } z = 0 \text{ for } 0 < x < 1, \tag{39}$$

$$V_z = F_x + ik^2W \quad \text{at } z = 0 \text{ for } 0 < x < 1, \tag{40}$$

$$U_z + W_x = -iF \quad \text{at } z = 0 \text{ for } 0 < x < 1, \tag{41}$$

$$F_x = 0 \quad \text{at } z = 0,\ x = 0 \text{ and } x = 1. \tag{42}$$

Note that $\mathrm{Re}(c) = 0$ corresponds to a solution that propagates around the circumference with speed $1/2$. In fact, this formulation is incomplete, since it is well-known that prescribing (36), a no slip boundary condition, all the way up to a moving contact line (implicit in (42), which states that the contact angle remains at its static value), leads to a non-integrable singularity in the stress

at the contact line (see [7]). There are many ways of dealing with this difficulty, but the simplest is to use a modified boundary condition in a small neighbourhood of the moving contact line, of dimensionless extent ϵ, and specify that the contact angle remains constant, so that (42) remains valid. Then, the contact angle measured some small distance much greater than ϵ from the contact line (the apparent contact angle) is significantly different from the static contact angle because viscous normal stresses in the neighbourhood of the contact line cause significant bending of the interface (see [8]).

We can see how these ideas can be applied to our problem by considering the asymptotic solution in the neighbourhood of a contact line.

2.1.2 Local solution

In terms of polar coordinates with origin at $x = z = 0$, with the solid wall, $x = 0$, at $\theta = 0$ and the free surface, $z = 0$, at $\theta = \pi/2$, we can write the linear stability problem as

$$\nabla \cdot \mathbf{U} = iV, \tag{43}$$

$$\nabla^2 \mathbf{U} - k^2 \mathbf{U} - \nabla P = 0, \tag{44}$$

$$\nabla^2 V - k^2 V + ik^2 P = 0, \tag{45}$$

for $0 < \theta < \pi/2$, where $\mathbf{U} = (U, W)$. Writing the polar components of $\mathbf{U}$ as U_θ and U_r, the local boundary conditions are, at $\theta = \pi/2$,

$$U_\theta = (c - ir)F, \tag{46}$$

$$\frac{1}{r}\frac{\partial V}{\partial \theta} = \frac{dF}{dr} + ik^2 U_\theta, \tag{47}$$

$$\frac{1}{r}\frac{\partial U_r}{\partial \theta} + \frac{\partial U_\theta}{\partial r} = -iF, \tag{48}$$

$$P = \frac{2}{r}\frac{\partial U_\theta}{\partial \theta} - \frac{1}{k\mathrm{Ca}}\left(\frac{d^2F}{dr^2} - k^2 F\right), \tag{49}$$

and

$$U_r = U_\theta = V = 0 \quad \text{at } \theta = 0. \tag{50}$$

We find that a suitable local asymptotic expansion, valid for $r \ll 1$, takes the form

$$U_\theta = U_{\theta 0}(\theta) + r \log r U_{\theta 1}(\theta) + r U_{\theta 2}(\theta) + \ldots,$$

$$U_r = U_{r0}(\theta) + \ldots,$$

$$V = r(\log r)^2 V_0(\theta) + r \log r V_1(\theta) + r V_2(\theta) + \ldots,$$

$$P = r^{-1} P_0(\theta) + \ldots,$$

$$F = F_0 + r \log r F_1 + r F_2 + \ldots$$

The nonintegrable singularity in the pressure as $r \to 0$ is a consequence of the moving contact line and the no slip boundary condition. If we substitute these expansions into (43) to (50), we can determine the functions of θ in the expansions. The key result is that

$$F \sim F(0)\left\{1 + \frac{2}{\pi}\left(2 + \frac{\pi^2}{4}\right) k\,\mathrm{Ca}\, c\,(r \log r + r)\right\} + ar \quad \text{as } r \to 0, \tag{51}$$

for some constant a.

Note that the slope of the contact line is of $O(\log r)$ as $r \to 0$. This is consistent with the results presented by Cox (1986) [8]. He showed that, if the capillary number is sufficiently small, the asymptotic solution given by (51) can be matched directly to an inner region where slip occurs. Since we are pursuing a linear stability analysis, the capillary number associated with the velocity of the contact line (not Ca) is arbitrarily small, and Cox's two region asymptotic analysis applies here. If the size of the inner, slip region is ϵ, we need

$$\frac{dF}{dr}(\epsilon) = 0,$$

and hence

$$a = -\frac{2}{\pi}\left(2 + \frac{\pi^2}{4}\right) F(0) k \,\mathrm{Ca}\, c \left(\log \epsilon + 2\right).$$

This means, noting that $r = x$ at $z = 0$, that

$$F \sim F(0)\left\{1 + \frac{2}{\pi}\left(2 + \frac{\pi^2}{4}\right) k \,\mathrm{Ca}\, cx \left(\log(x/\epsilon) - 1\right)\right\} \quad \text{as } x \to 0. \tag{52}$$

This is the boundary condition that we will use instead of (42). In the following computations, we used $\epsilon = 10^{-5}$. The solution did not seem very sensitive to changes in ϵ in a few test cases that we tried.

2.1.3 Numerical solution of the linear stability problem: finite difference method

We aim to solve the eigenvalue problem given by (32) to (41) and (52) using a finite difference discretization of the governing equations. We begin by truncating the semi-infinite domain of solution to the rectangle $0 < x < 1$ and $-L < z < 0$, and choose $L > 0$ sufficiently large that the solution converges, replacing (37) with

$$U = V = W = 0 \quad \text{at } z = -L \text{ for } 0 < x < 1. \tag{53}$$

Since (32), (33) and (35) are the two-dimensional Stokes equations with a source of mass due to the crossflow, we anticipate that we will need to use a staggered grid. We locate the discretized velocities, U, V and W, at the x-edges, centres and z-edges respectively of cells with corners $x = x_i$ for $i = 1, 2, \ldots, N$ and $z = z_j$ for $j = 1, 2, \ldots, M$, as shown in figure 3. We will not assume that the grid is uniform, but we will need $x_1 = 0$, $x_N = 1$, $z_1 = -L$ and $z_{M-1} + z_M = 0$. The discretized pressure is located at the centre of each cell, as is the discretized position of the free surface along the line $z = 0$. In addition, we require ghost points that lie outside the domain of solution, in order to be able to implement the boundary conditions. Specifically, we need ghost values of F and V at the x-boundaries, ghost values of U at the boundary $z = -L$ and ghost values of W at the boundary $z = 0$. This is all easier to see in figure 3.

With the unknowns discretized in this manner, it is straightforward to discretize the governing equations and boundary conditions. This gives us a set of linear equations that can be written in matrix-vector form as a generalized eigenvalue problem, $(A - Bc)y = 0$. We set up the matrices A and B in MATLAB in sparse form. For given k and Ca, we can calculate the eigenvalues, c, and associated eigenvectors, y, very efficiently with the MATLAB routine `eigs`, which uses an iterative method optimized for sparse matrices.

In the results shown below, we used a grid with spacing 10^{-3} in the x-direction close to the contact lines, increasing gradually to 10^{-2} away from the contact lines. In total, there are 130

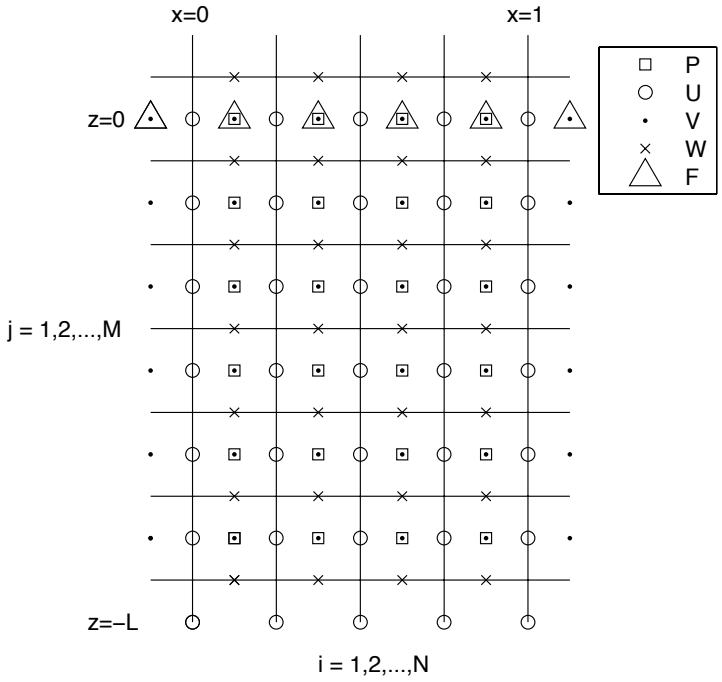

Figure 3: The discretization of the linear stability problem.

cells in the x-direction. Similarly, in the z-direction, the grid spacing is 10^{-3} at the free surface, gradually increasing to 0.25 for larger z. We also found that we needed to reduce the z-grid spacing close to the boundary $z = -L$ to achieve a converged solution. In total, there are 143 cells in the z-direction. We performed several grid refinement tests to check that the solution had converged.

Figure 4 shows how the real and imaginary parts of the first few eigenvalues c_i vary with k for $\mathrm{Ca} = 0.6$. The eigenvalues and corresponding eigensolutions seem to be of two types.

Firstly, there is a sequence of eigenvalues with negative real part. These are stable eigenmodes that move at the mean value of the velocities of the walls ($\mathrm{Im}(c) = 1/2$) for $k < k_H \approx 6.17$. It is easiest to visualise this in terms of plane Couette flow with the walls moving at equal speeds in opposite directions. These stable eigenmodes then do not move with either wall, and decay exponentially with time. At $k = k_H$ there is a Hopf bifurcation. For $k > k_H$, the real parts of the first two stable eigenmodes become equal, and their imaginary parts deviate from $1/2$, which indicates the formation of an oscillatory mode. We would expect a sequence of such bifurcations as k increases. Some typical eigensolutions of this first type are shown in figures 5 and 6. Note that the contact lines are not displaced from zero in these eigensolutions. As we would expect, the number of zeros of F increases by one with each successive eigenvalue.

Secondly, there are two neutral eigenmodes with zero real part, which are mirror images about the centre line, $x = 1/2$. These neither grow nor decay in this linear approximation. One mode has imaginary part i, and one zero. When k is moderately large, each mode is localized at one of the walls, and moves with that wall. For smaller values of k, the eigenmode does not look very different to the stable eigenmodes shown in figures 5 and 5. However, the key difference is that the neutrally-stable eigenmodes have a nonzero contact line displacement. Some typical eigensolutions of this second type are shown in figure 7.

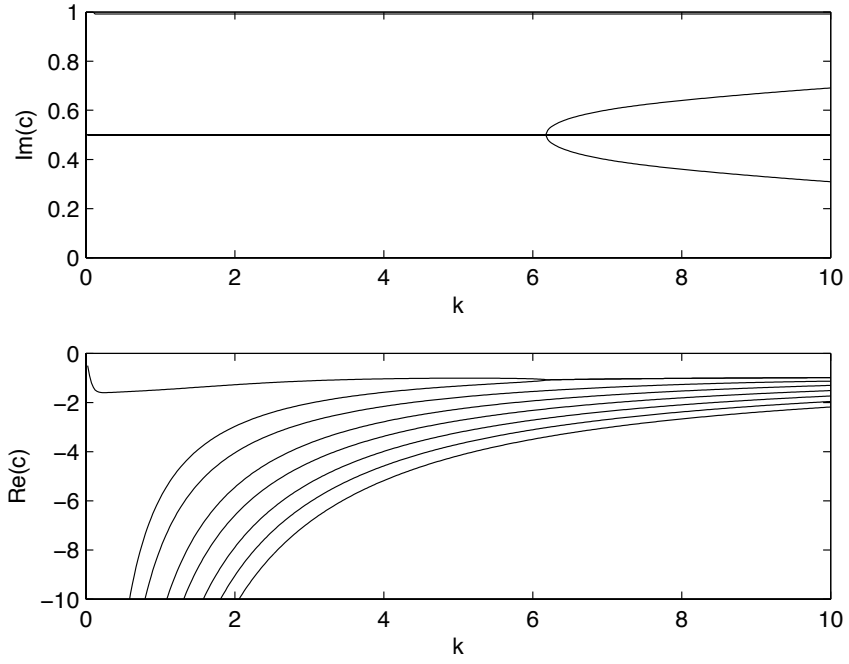

Figure 4: The real and imaginary parts of the first 10 eigenvalues.

Although this is about as clear a result as can be expected from a numerical solution, it is rather unsatisfactory, as it leaves the question of the stability of the flow unanswered. Since there are two neutrally-stable modes, their long time behaviour can only be determined by using a weakly-nonlinear analysis. The linear analysis says that, from any small initial perturbation of the flow that displaces the contact lines, the contact lines will not move, and only the neutrally-stable eigenmodes will remain[3]. A weakly nonlinear analysis is very challenging, and remains to be attempted.

3 Cylindrical Geometry

3.1 Derivation of small-gap equations

To describe the flow within the gap between two concentric cylinders, we introduce the coordinate system shown in figure 1c, where the fluid is found in the domain $R < r < R + d, 0 \leq \theta < 2\pi, z < F(r, \theta, t)$. The equations of motion for the fluid are given by the continuity equation

$$\frac{1}{r}\left[ru\right]_r + \frac{1}{r}v_\theta + w_z = 0 \ , \tag{54}$$

where $\mathbf{u} = u(r, \theta, z, t)\mathbf{r} + v(r, \theta, z, t)\boldsymbol{\theta} + w(r, \theta, z, t)\mathbf{z}$ is the fluid velocity, and $\mathbf{r}, \boldsymbol{\theta}, \mathbf{z}$ are unit vectors in the corresponding cylindrical coordinates r, θ, z. The Navier-Stokes equations denote the

[3]In addition, it is somewhat troubling that numerical attempts to find solutions to (35) – (41) using femlab to solve the PDEs coupled with matlab to minimize the error made with various choices for F at $z = 0$ and P at $x = 0$ and $x = 1$ did not find satisfactory solutions.

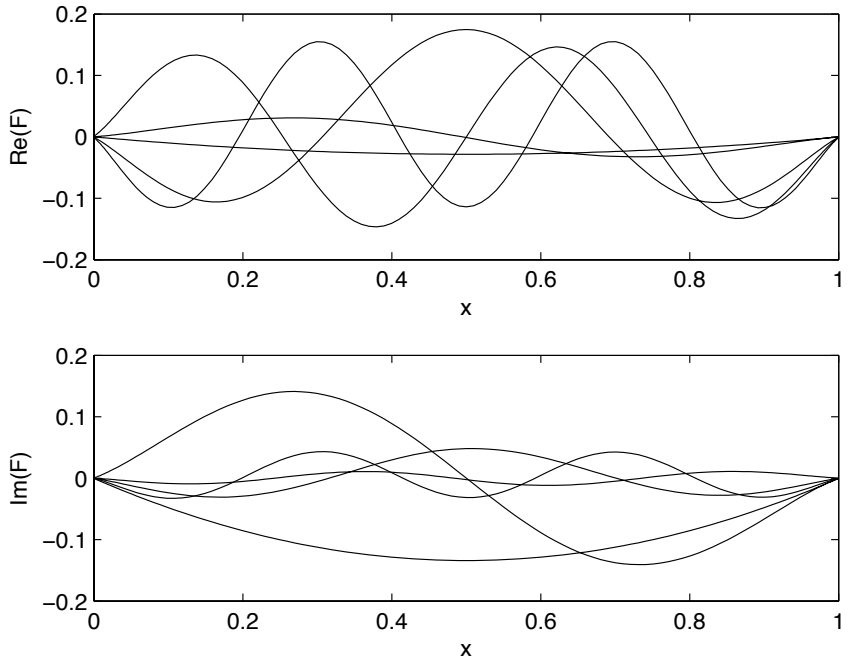

Figure 5: The free surface displacement of the first 5 stable eigenmodes for Ca = 0.6, $k = 0.1$.

conservation of momentum of the fluid in each direction:

$$\rho\left\{u_t + uu_r + \frac{1}{r}vu_\theta + wu_z - \frac{v^2}{r}\right\} = -p_r + \mu\left\{\nabla^2 u - \frac{u}{r^2} - 2\frac{v_\theta}{r^2}\right\} \quad (55)$$

$$\rho\left\{v_t + uv_r + \frac{1}{r}vv_\theta + wv_z + \frac{uv}{r}\right\} = -\frac{1}{r}p_\theta + \mu\left\{\nabla^2 v + \frac{2}{r^2}u_\theta - \frac{v}{r^2}\right\} \quad (56)$$

$$\rho\left\{w_t + uw_r + \frac{1}{r}vw_\theta + ww_z\right\} = -p_z + \mu\nabla^2 w \ , \quad (57)$$

where ρ is the fluid density, p is the fluid pressure, μ is the fluid dynamic viscosity, ∇^2 is the standard Laplacian in cylindrical coordinates.

For the boundary conditions, some care is needed local to the contact lines where the fluid interface meets the inner and outer cylinder. We address this issue separately, but apply away from the free surface the no-slip boundary condition along each cylinder

$$r = R: \qquad u = v = w = 0 \quad (58)$$

$$r = R + d \qquad u = w = 0 \ , \ v = U_o \ . \quad (59)$$

Far from the free surface $z \to \infty$, we shall apply matching conditions, which we neglect at this stage of the model development.

At the free surface $z = F(r, \theta, t)$, we apply the kinematic boundary condition, normal fluid stresses are balanced by capillary effects, and the shear stress in the azimuthal and radial directions

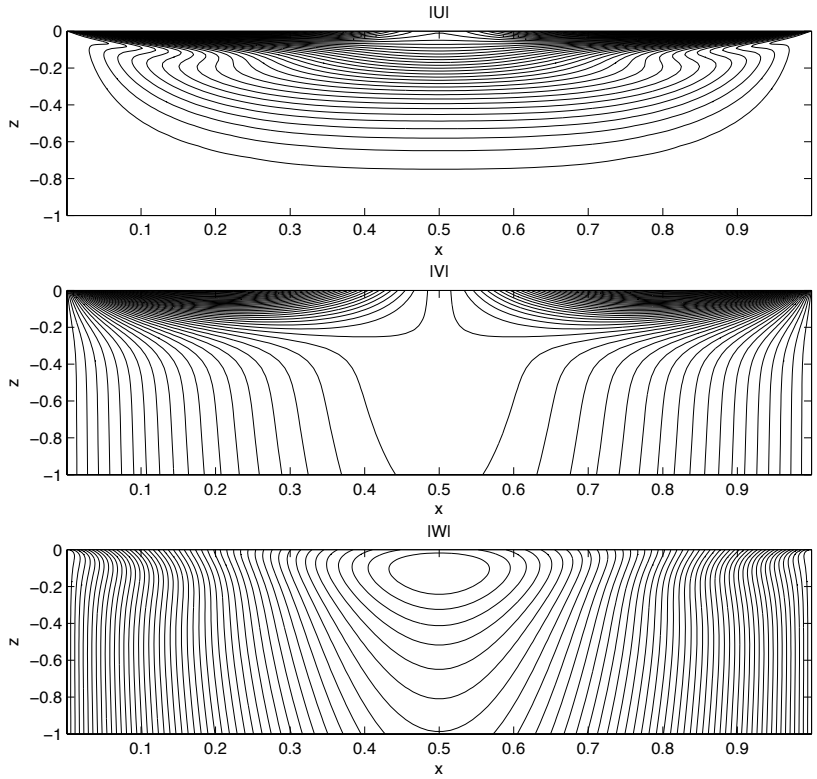

Figure 6: The velocity field of the first stable eigenmode for Ca = 0.6, $k = 0.1$.

along the free surface vanish. Thus, given the stress tensor of the fluid $\mathbf{T}$,

$$\mathbf{T} = -p\mathbf{I} + 2\mu \begin{bmatrix} u_r & \frac{r}{2}(\frac{v}{r})_r + \frac{1}{2r}u_\theta & \frac{1}{2}(u_z + w_r) \\ \frac{r}{2}(\frac{v}{r})_r + \frac{1}{2r}u_\theta & \frac{1}{r}v_\theta + \frac{u}{r} & \frac{1}{2}(\frac{1}{r}w_\theta + v_z) \\ \frac{1}{2}(u_z + w_r) & \frac{1}{2}(\frac{1}{r}w_\theta + v_z) & w_z \end{bmatrix} ,$$

where $\mathbf{I}$ is the identity matrix, we find that at $z = F(r, \theta, t)$;

$$F_t + uF_x + \frac{v}{r}F_\theta - w = 0 \tag{60}$$

$$\mathbf{n} \cdot \mathbf{T} \cdot \mathbf{n} = \sigma\kappa \tag{61}$$

$$(\mathbf{T} \cdot \mathbf{n}) \times \mathbf{n} = 0 \tag{62}$$

where $\mathbf{n} = \nabla [z - F(r, \theta, t)]$ and $\kappa = \nabla \cdot \mathbf{n}$ is twice the mean curvature.

We use the following scales, where $[f]$ give the scale of the quantity f,

$$r = R + xd \ , \ [z] = d \ , \ [v] = U_o, [u, w] = \frac{d}{R} U_o \ , \ [t] = \frac{R}{U_o} \ , \ [p] = \frac{\mu U_o}{R} \ ,$$

to find the following nondimensional version of the fluid flow (N.B. all variables are now the nondi-

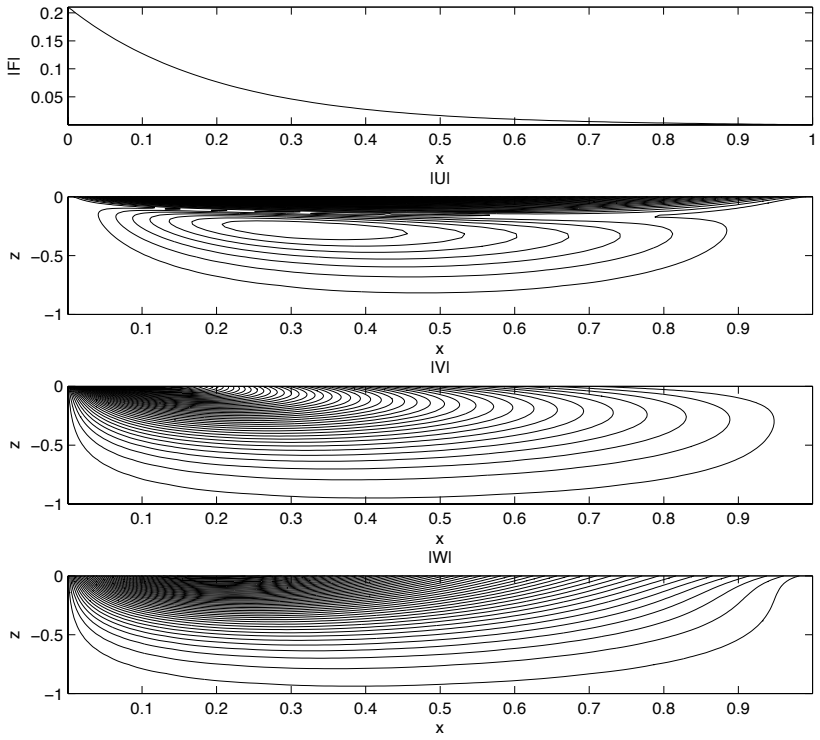

Figure 7: A neutrally-stable eigenmode for Ca = 0.6, $k = 5$.

mensional counterparts of the dimensional versions above):

$$\frac{1}{1+\epsilon x}\left[(1+\epsilon x)u\right]_x + \frac{1}{1+\epsilon x}v_\theta + w_z = 0 \tag{63}$$

$$\mathrm{Re}\left\{\epsilon\left(u_t + uu_x + \frac{v\,u_\theta}{1+\epsilon x} + wu_z\right) - \frac{v^2}{1+\epsilon x}\right\} = -p_r + \left\{\nabla^2 u - \frac{\epsilon^2 u}{(1+\epsilon x)^2} - \frac{2\epsilon\, v_\theta}{(1+\epsilon x)^2}\right\} \tag{64}$$

$$\mathrm{Re}\left\{v_t + uv_x + \frac{1}{1+\epsilon x}vv_\theta + wv_z + \frac{\epsilon\, uv}{1+\epsilon x}\right\} = -\frac{\epsilon\, p_\theta}{1+\epsilon x} + \left\{\nabla^2 v + \frac{2\epsilon^3\, u_\theta}{(1+\epsilon x)^2} - \frac{\epsilon v}{(1+\epsilon x)^2}\right\} \tag{65}$$

$$\epsilon\mathrm{Re}\left\{w_t + uw_x + \frac{vw_\theta}{1+\epsilon x} + ww_z\right\} = -p_z + \nabla^2 w\ , \tag{66}$$

where $\epsilon = d/R$ is the aspect ratio, $\mathrm{Re} = U_o d/\nu$ is the reduced Reynolds number of the fluid, and

$$\nabla^2 f = \frac{1}{1+\epsilon x}\left\{(1+\epsilon x)f_x\right\}_x + f_{zz} + \frac{\epsilon^2}{(1+\epsilon x)^2}f_{\theta\theta}\ ,$$

is the scaled version of the Laplacian.

The boundary conditions (60-62) remain unchanged with the exception that

$$r = 1 + \epsilon x \ , \ \mathbf{n} = \frac{-F_x \mathbf{x} - \frac{\epsilon}{r} F_\theta \, \boldsymbol{\theta} + \mathbf{z}}{\sqrt{F_x^2 + \left(\frac{\epsilon}{r} F_\theta\right)^2 + 1}} \ .$$

Note that from this scaling, a capillary number $\mathrm{Ca} = \mu U_o / \sigma$ is introduced. From the scales of the problem, $\epsilon \approx 1/10, \mathrm{Re} \approx 6, \mathrm{Ca} \approx 1/10$.

We consider the effective equations of motion in the limit $\epsilon \to 0$. In this limit, we find that the problem reduces to

$$u_x + v_\theta + w_z = 0 \tag{67}$$

$$\begin{aligned} \nabla^2 u - p_x &= -\mathrm{Re}\, v^2 && (68)\\ \nabla^2 v &= \mathrm{Re}\, \{v_t + u v_x + v v_\theta + w v_z\} && (69)\\ \nabla^2 w - p_z &= 0 && (70) \end{aligned}$$

where $\nabla^2 f = f_{xx} + f_{zz}$, and subject to the boundary conditions

$$\begin{aligned} \underline{x = 0}: &\quad u = 0 \ , \ v = 0 \ , \ w = 0 && (71)\\ \underline{x = 1}: &\quad u = 0 \ , \ v = 1 \ , \ w = 0 && (72)\\ \underline{z = F(x,\theta,t)}: &\quad F_t + u F_x + v F_\theta - w = 0 && (73)\\ &\quad -p + 2\left\{u_x F_x^2 - (u_z + w_x) F_x + w_z\right\} = \frac{1}{\mathrm{Ca}} F_{xx} && (74)\\ &\quad v_z - v_x F_x = 0 && (75)\\ &\quad (u_z + w_x)(1 - F_x^2) = 2 u_x F_x + v_x F_\theta (1 + F_x^2) - 2 w_z F_x && (76) \end{aligned}$$

Note that the classical Taylor-Couette flow solution $u = w = 0, v = V(x)$ is not necessarily a solution to this problem due to the stress conditions at the free surface. We thus need to consider the solutions to this problem in limiting cases. At the workshop, the only case that was considered was $\mathrm{Re} = 0$. In this limit, if $F = 0$, then the base-state solution $u = w = 0, v = x$ satisfies (67)-(70) and all of the boundary conditions (73)-(76).

3.2 Linear Stability Theory, $\mathrm{Re} = 0$

To test the linear stability of this base-state solution to (67)-(70) subject to the boundary conditions (73)-(76), we apply the following ansatz

$$\begin{aligned} u &= \delta\left\{\hat{U}(x,z) e^{-ik\theta + ct} + c.c.\right\} && (77)\\ v &= x + \delta\left\{\hat{V}(x,z) e^{-ik\theta + ct} + c.c.\right\} && (78)\\ w &= \delta\left\{\hat{W}(x,z) e^{-ik\theta + ct} + c.c.\right\} && (79)\\ p &= \delta\left\{\hat{P}(x,z) e^{-ik\theta + ct} + c.c.\right\} && (80)\\ F &= \delta\left\{\hat{F}(x) e^{-ik\theta + ct} + c.c.\right\} && (81) \end{aligned}$$

where $\delta \ll 1$ is an amplitude scale, k is the wavenumber, c is a complex growth rate, and *c.c.* denotes the complex conjugate of the previous term. By substituting (77)-(81) into the equations

(67)-(70) along with the boundary conditions (73)-(76), we arrive at the following system to be solved

$$\begin{aligned}
\hat{U}_x - i\,k\,\hat{V} + \hat{W}_z &= 0 && (82)\\
\hat{U}_{xx} + \hat{U}_{zz} - \hat{P}_x &= 0 && (83)\\
\hat{V}_{xx} + \hat{V}_{zz} &= 0 && (84)\\
\hat{W}_{xx} + \hat{W}_{zz} - \hat{P}_z &= 0 && (85)\\
& && (86)
\end{aligned}$$

$$\begin{aligned}
\underline{x=0}: \quad & \hat{U} = \hat{V} = \hat{W} = 0 && (87)\\
\underline{x=1}: \quad & \hat{U} = \hat{V} = \hat{W} = 0 && (88)\\
\underline{z=0}: \quad & (c - ikx)\,\hat{F} = \hat{W} && (89)\\
& -\hat{P} + 2\hat{W}_z = \frac{1}{\mathrm{Ca}}\,\hat{F}_{xx} && (90)\\
& \hat{U}_z + \hat{W}_x = -i\,k\,\hat{F} && (91)\\
& \hat{V}_z = \hat{F}_x\ . && (92)
\end{aligned}$$

along with the condions that $\hat{U}, \hat{V}, \hat{W} \to 0$ as $z \to -\infty$.

Note that k can be scaled from this set of equations by the definition

$$\hat{U} = k\,U\ , \hat{V} = V\ , \hat{W} = k\,W\ , \hat{P} = k\,P\ ,$$

which gives the final set of equations and boundary conditions to be considered:

$$\begin{aligned}
U_x - i\,V + W_z &= 0 && (93)\\
\hat{U}_{xx} + \hat{U}_{zz} - \hat{P}_x &= 0 && (94)\\
\hat{V}_{xx} + \hat{V}_{zz} &= 0 && (95)\\
\hat{W}_{xx} + \hat{W}_{zz} - \hat{P}_z &= 0 && (96)\\
& && (97)
\end{aligned}$$

$$\begin{aligned}
\underline{x=0}: \quad & U = V = W = 0 && (98)\\
\underline{x=1}: \quad & U = V = W = 0 && (99)\\
\underline{z=0}: \quad & i\ (c - ix)\,\hat{F} = W && (100)\\
& -\hat{P} + 2\hat{W}_z = \frac{1}{k\,\mathrm{Ca}}\,\hat{F}_{xx} && (101)\\
& \hat{U}_z + \hat{W}_x = -i\,\hat{F} && (102)\\
& \hat{V}_z = F_x\ . && (103)
\end{aligned}$$

along with the conditions that $U, V, W \to 0$ as $z \to -\infty$. This problem now depends only on one parameter $\bar{\mathrm{Ca}} = k\,\mathrm{Ca}$, and is equivalent to the small wavenumber, large capillary number expansion of the slot geometry problem (21)-(30).

In the following figure, we plot the growth rates as a function of the combined Capillary number $\bar{\mathrm{Ca}}$. Note that as in the slot geometry case, all of the modes considered are stable.

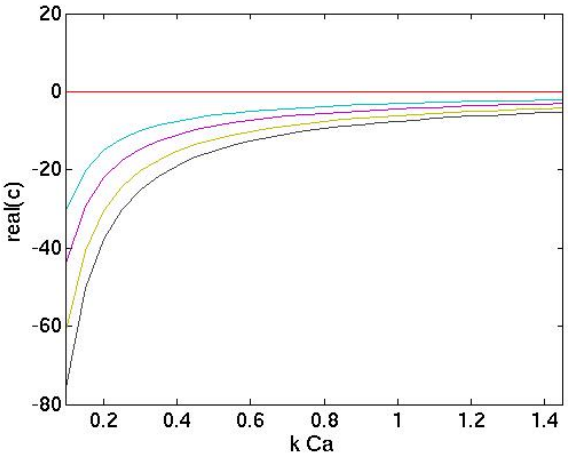

Figure 8: Growth rates of cylindrical problem in the small-gap limit as a function of kCa. Note that the growth rates are always negative for all capillary numbers considered.

4 Conclusions

In this report, we investigated the linear stability of two different geometric models of the meniscus region of a fluid-dynamic bearing of a hard disk drive. Previous inviscid results [4] reported an instability for the slot geometry when inertial effects dominate over capillary effects. We found, in the limit when viscous effects dominate of inertial effects, including contact-line condtions at the gas-liquid-solid trijunctions, that the flat meniscus is stable. In the cylindrical geometry, the inviscid analysis results in a non-trivial base-state solution, and its stability was not considered here. The case when viscous effects dominate inertial effects for the cylindrical model results in a stable interfacial problem.

Extensions to this work will need to include the regime when viscous effects and inertial effects are comparable. Our numerical method above can be extended relatively straight-forwardly for the slot geometry problem. We intend on continuing this inquiry in this direction.

Appendix

Here we consider the inviscid analysis of the cylindrical problem. If we use the following scales,

$$[u, v, w] = R\Omega, [r, z] = R, [t] = 1/\Omega, [p] = \rho(R\Omega)^2 \ ,$$

then the problem reduces to, in the limit of $Re \to \infty$,

$$\begin{aligned}
\frac{1}{r}\frac{\partial}{\partial r}\left[ru\right] + \frac{1}{r}\frac{\partial v}{\partial \theta} + \frac{\partial w}{\partial z} &= 0 \\
u_t + uu_r + \frac{1}{r}vu_\theta + wu_z - \frac{v^2}{r} + p_r &= 0 \\
v_t + uv_r + \frac{1}{r}vv_\theta + wv_z + \frac{uv}{r} + \frac{1}{r}p_\theta &= 0 \\
w_t + uw_r + \frac{1}{r}vw_\theta + ww_z + p_z + \frac{1}{Fr} &= 0 \ .
\end{aligned}$$

on $z < \epsilon f(r,\theta,t)$ and $1 < r < 1+\epsilon$. The boundary conditions are no penetration along the cylinder walls $u = 0$ on $r = 1, 1+\epsilon$, and along the free surface $z = \epsilon f(r,\theta,t)$:

$$\begin{aligned} f_t + u f_r + v f_\theta - w &= 0 \\ p &= -\frac{Fr}{Bo}\kappa \ , \end{aligned}$$

where hydrostatics near the free-surface have been neglected. If we assume that the steady base-state is θ-independent, then $u = w = 0$, and the radial momentum equation results

$$p_r = \frac{v^2}{r} \ .$$

Extending this to the free surface and applying the normal stress condition provides the compatability condition (1) for the free surface as described in the Introduction.

References

[1] W.C. Blount, "Fluid Dynamic Bearing Spindle Motors: Their future in hard disk drives", IBM Corporation White Ppaer, IBM Storage Systems Group, San Jose, CA. 95193.

[2] "Free surface cusp formation as a failure mechanism for hard disk drives with fluid dynamic bearings", Billingham et al., Proceedings of the Twentieth Annual Workshop on Mathematical Problems from Industry, Department of Mathematical Sciences, University of Delaware, Newark, DE, 2004.

[3] F. Hendriks, B.S. Tilley, J. Billingham, P. Dellar, and R. Hinch, "Dynamics of the Oil-Air Interface in Hard Disk Drive Bearings", *IEEE Trans. on Magnetics*, **41** (10) 2884-2886: (2005).

[4] J.S. Walker, G. Talmage, S.H. Brown, and N.A. Sondergaard, "Kelvin-Helmholtz instability of Couette flow between vertical walls with a free surface", *Phys. Fluids A*, **5** (6) 1468-1471: (1993).

[5] *Fundamentals of Two-Fluid Dynamics. Part 1: Mathematical Theory and Applications*, D.D. Joseph and Y.Y. Renardy (Springer-Verlag, New York, 1993).

[6] G. Baier and M.D. Graham, "Two-fluid Taylor-Couette flow with countercurrent axial flow: Linear theory for immiscible liquids between corotating cylinders", *Phys. Fluids* **12** (2) 294-303: (2000).

[7] E.B. Dussan V. and S.H. Davis, "On the motion of a fluid-fluid interface along a solid surface", *J. Fluid Mech.* **65** 71-95: (1974).

[8] R.G. Cox, "The dynamics of the spreading of liquids on a solid surface. Part I. Viscous flow.", *J. Fluid Mech.* **168** 169-194: (1986).